



Effects of alloying elements on thermal conductivity of pearlitic gray cast iron

Gui-quan Wang^{1,2} · Xiang Chen^{1,3} · Yan-xiang Li^{1,3} · Yuan Liu^{1,3} · Hua-wei Zhang^{1,3} · Zhong-li Liu²

Received: 22 May 2018 / Revised: 23 July 2018 / Accepted: 25 July 2018 / Published online: 31 August 2019
© China Iron and Steel Research Institute Group 2019

Abstract

A quantitative model is proposed to describe the thermal conductivity of alloyed pearlitic gray cast iron. The model is built by combining the computational thermodynamics and effective medium theory. The volume fractions and concentrations of precipitated phases in as-cast structure are estimated in consideration of partial and para-equilibrium. The conductivity of alloyed ferrite is calculated, taking into account the electronic and vibrational contributions of alloying elements. The model provides a good agreement with microstructure analysis and measured thermal conductivity. The influence of common alloying elements was discussed from the viewpoint of precipitation of phases and scattering of alloying atoms. This model can also be used as a numerical tool for designing the pearlitic gray cast irons with high thermal conductivity and high tensile strength.

Keywords Thermal conductivity · Thermodynamic model · Gray cast iron · Alloying element

1 Introduction

Gray cast iron has been widely used in the manufacture of structural components subjected to thermal cycling [1–4], such as permanent molds, cylinder heads and brake disks. Thermal stresses of these components caused by thermal expansion and contraction during thermal cycling are determined by the heat conducting capability. Thus, thermal conductivity is an important property for gray cast iron.

A great number of studies concerning the thermal conductivity of gray cast iron have been carried out in practical measurements [5–10]. It is clear that, at a certain temperature, thermal conductivity of gray cast iron depends on the composition and structural features, which mainly include the morphology of graphite and the type of matrix. Since a

homogeneous structure, including A-type graphite and pearlitic matrix, is preferred in most applications due to its optimum comprehensive mechanical and thermal properties and can be obtained by a reliable inoculation [11, 12], how to study the influence of chemical composition is thus the main question to be answered. There are also extensive investigations on the effects of specific elements in experiments [13]; however, these data can only provide qualitative analysis due to the ambiguous experimental procedure, indistinct graphite morphology and neglecting of comprehensive effects of multiple elements.

In order to develop quantitative solutions, two typical methods, i.e., the regression model and the average field approach, have been developed to calculate the thermal conductivity of cast iron. Based on the vast experiment data, regression models can be built by the direct rule of mixture without assumptions [8, 14]. The expressions of those models usually include many parameters representing the influence of microstructure and composition. In another model, which is developed by Helsing and Grimvall [15], gray cast iron is considered as a composite consisting of pearlite, graphite and cementite. The contribution of all phases to thermal conductivity is described by the effective medium theory. However, both methods mentioned above cannot be expediently utilized for the

✉ Xiang Chen
xchen@tsinghua.edu.cn

¹ School of Materials Science and Engineering, Tsinghua University, Beijing 100084, China

² School of Nuclear Equipment and Nuclear Engineering, Yantai University, Yantai 264005, Shandong, China

³ Key Laboratory for Advanced Materials Processing Technology, Tsinghua University, Beijing 100084, China

designing of gray cast iron. The downside of the regression model is that its accuracy relies heavily on the amount of data and the condition of experiment. If the data set is too small or the experimental condition is too narrow, the model will not be commonly applied. The average field approximation is more flexible and can be applied to different microstructural features. However, it is time-consuming that the microstructural features should be measured accurately for each composition. Moreover, it also cannot completely reflect the effects of alloying elements since the model was built without discussing how the microstructure relied on the composition.

The main objective of the present paper is to provide a more comprehensive model to systematically study the effects of alloying elements on the thermal conductivity of pearlitic gray cast irons. On the basis of Thermo-Calc software, the information on as-cast microstructure was predicted by combining thermodynamics method with micro-segregation models. The total thermal conductivity was then calculated using an effective medium approximation. Calculations of the model were compared with the experimental measurements. The influence of various elements on total thermal conductivity was also discussed based on the calculation.

2 Numerical algorithms

In order to estimate the effects of alloying elements, the model was built mainly based on two considerations: the precipitation of phases due to compositional changing and the inherent thermal conductivity of various phases. The present model can thus be divided into two parts: computational thermodynamics and effective medium theory. The morphology of graphite is assumed to be available since it can be considered stable for a certain reliable inoculation process. The microstructural information, including volume fractions and concentrations of precipitated phases, was calculated in thermodynamic part by following the transformation path for a given multi-component system. On the basis of these results, the thermal conductivity of alloyed ferrite is calculated at room temperature. Then, the effective thermal conductivity of gray cast iron is solved by effective medium theory. The schematic of numerical schemes is shown in Fig. 1.

2.1 Computational thermodynamics

For a normal cooling rate in sand mold, it can be approximated that the behavior of a solidifying system is controlled by the thermodynamical properties and solute diffusion in phases [16]. Additionally, with an effective inoculation, the solidification process of gray cast iron can

be considered to consist of primary precipitation (for hypoeutectic or hypereutectic irons), stable eutectic transformation, decarburization of austenite and metastable eutectoid [17].

In the present model, considering that the diffusion of C is much faster than that of the other elements (Si, Mn, Mo, etc.), partial equilibrium (PE) and para-equilibrium (PA) models were used to simulate the solute diffusion for solidification and solid-state transformation, respectively [18, 19]. In PE model, it is assumed that C diffuses completely in both liquid and solid, while other elements just diffuse in the liquid. In PA model, the chemical potential of C among solid phases is considered equal, while the condition on substitutional elements is calculated by the summation of the product of the average chemical potential and the average ubiquitous fraction (u-fraction) [19, 20]. Initial mole fraction (X_i^0) of component i , total amount of atoms ($N = 1$), start/stop temperature ($T_{\text{start}}/T_{\text{end}}$) and temperature step (ΔT) are defined as the initial conditions. With the decreasing temperature, the phase equilibrium of a given multi-component system is calculated at each temperature step k . The information on each phase $j = [1, m]$, including its amount (${}^kN^j$) and concentration (${}^kX_i^j$), is then recalculated by the corresponding model. It should be noted that, even though there is a solute distribution for substitutional elements in solids due to neglecting their diffusion completely, an average solid composition ${}^k_{\text{EQ}}\bar{X}_i^{j \neq L}$ and mole fraction ${}^k_{\text{EQ}}N_i^{j \neq L}$ are used before the recalculation was performed (as shown in Fig. 1). The left subscript EQ represents the corresponding value before recalculation, while the right superscript L means the liquid. This approximation makes the calculation of thermal conductivity of ferrite feasible, and fortunately, it also makes the calculation better agree with the measurements because of the limited diffusion of substitutional elements in a real alloy. Then, the PE or PA model is performed to simulate the micro-segregation depending on whether the liquid has been exhausted. The volume fractions (V^j) of phases are also estimated at each step. Main analytical equations of these models are shown in Fig. 1.

2.2 Effective medium theory

The microstructural constituents, including pearlite (P), A-type graphite (G) and eutectic cementite (E), are concerned. Pearlite can also be considered as the composite of ferrite (F) and eutectoid cementite (C).

2.2.1 Ferrite

The total thermal conductivity of ferrite can be considered as the summation of lattice conduction and electron

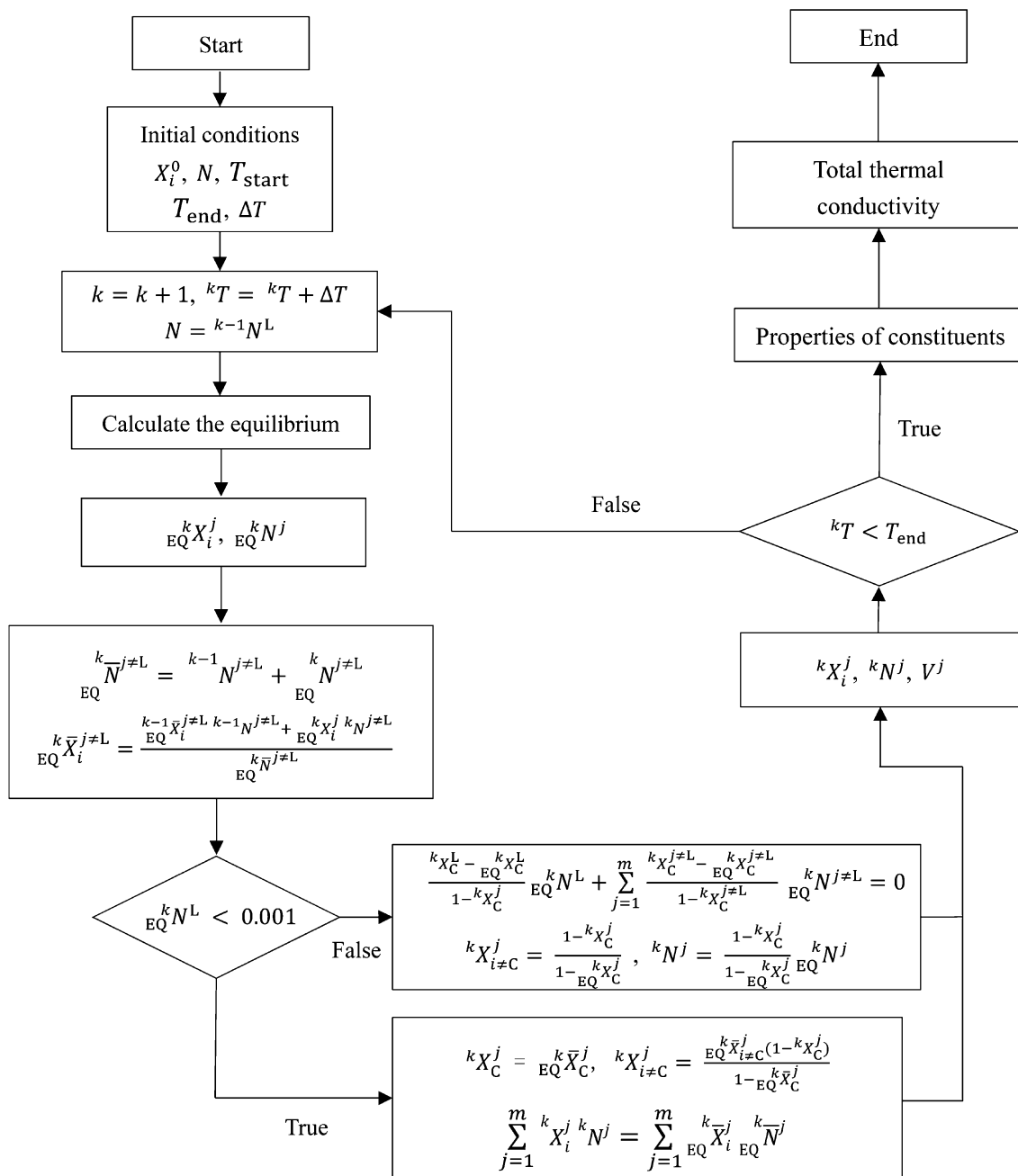


Fig. 1 Schematic of numerical schemes accounting for a combination of computational thermodynamics and effective medium approximation

conduction. Based on the previous work, the thermal conductivity of alloyed ferrite (λ_F) can be estimated by [15]

$$\lambda_F = \left(\frac{1}{\lambda_{\alpha,Fe}} + \sum_i A_i X_i^F \right)^{-1} + \left(\frac{\rho_{Fe}}{L_e T} + \frac{1}{L_0 T} \sum_i \rho_i X_i^F \right)^{-1} \tag{1}$$

The first term on the right-hand side represents the contribution of lattice conduction, where $\lambda_{\alpha,Fe}$ is the lattice conductivity of pure ferrite, and the effect of elements is approximated as the summation of product of

corresponding mole fraction (X_i^F) and coefficients A_i . The second term expresses the electrical conduction, where T is the temperature in Kelvin, ρ_{Fe} stands for the electrical resistivity of pure ferrite, L_e and L_0 are the Lorenz number for pure and alloyed ferrite respectively and can be treated as constants at 300 K [$L_e = 2.03 \times 10^{-8}$ (W Ω K $^{-2}$), $L_0 = 2.44 \times 10^{-8}$ (W Ω K $^{-2}$)], and ρ_i is the relative electrical resistivity coefficients. Table 1 lists the A_i and ρ_i of alloying elements which are important for gray cast iron. All of them are obtained depending on the experimental

Table 1 Experimental values for coefficients A_i and ρ_i at 300 K [21–25]

Coefficient	Si	Mn	Cu	Mo	Ni	Cr
$A_i/(\text{mm K W}^{-1} \text{ at.}\%^{-1})$	8.1	2.2	9.1	13.0	4.1	0.2
$\rho_i/(\mu\Omega \text{ cm at.}\%^{-1})$	6.6	4.5	3.2	4.8	2.5	3.7

measurements [21–25]. Corresponding data of pure bcc Fe are given in Table 2.

2.2.2 Cementite and graphite

Holmgren [13] has summarized many known measured and estimated thermal conductivity of Fe_3C and graphite. The values used in the calculation are given in Table 2.

Graphite is a strongly anisotropic phase because of its hexagonal crystal lattice. The conductivity along the a -direction is considerably higher than the one along c -direction. It has been generally agreed that A-type graphite grows in the a -direction and thickens in the c -direction. In order to get the effective thermal conductivity, the lamellar graphite was assumed as oblate spheroid with major axis along x and y of lengths R and minor axis along z of thickness εR . ε is defined as the shape factor of graphite flake.

2.2.3 Pearlite

Pearlite can be considered as a separate anisotropic phase with ideal morphology, consisting of parallel alternating lamellae of ferrite and cementite. The thermal conductivity along the lamellae ($\lambda_{\parallel,\text{P}}$) and perpendicular to the lamellae ($\lambda_{\perp,\text{P}}$) can be estimated by [15]:

$$\lambda_{\parallel,\text{P}} = V^{\text{C}}\lambda_{\text{C}} + V^{\text{F}}\lambda_{\text{F}} \quad (2)$$

$$\lambda_{\perp,\text{P}} = (V^{\text{C}}/\lambda_{\text{C}} + V^{\text{F}}/\lambda_{\text{F}})^{-1}, \quad (3)$$

where V^{C} and V^{F} represent the volume fractions of eutectoid cementite and ferrite, respectively; and λ_{C} is the thermal conductivity of cementite. Thus, for pearlite grains

Table 2 Thermal conductivity (λ) and electrical resistivity (ρ) at 300 K [13, 15]

Phase	$\lambda/(\text{W m}^{-1} \text{ K}^{-1})$	$\rho/(\mu\Omega \text{ cm})$
Pure ferrite	78.5	10.0
Graphite (basal plane)	500.0	–
Graphite (prism plane)	10.0	–
Cementite	8.1	–

with random orientation, Eq. (4) [12] can be used to estimate the effective thermal conductivity (λ_{P}) of pearlite.

$$\lambda_{\text{P}} = \frac{1}{4} \left[\lambda_{\parallel,\text{P}} + \left(\lambda_{\parallel,\text{P}}^2 + 8\lambda_{\parallel,\text{P}}\lambda_{\perp,\text{P}} \right)^{1/2} \right]. \quad (4)$$

Finally, for a typical microstructure, consisting of weakly anisotropic pearlite grains, isotropic cementite phase and strongly anisotropic oblate spheroidal graphite, the total thermal conductivity (λ') of gray cast iron can be solved by [15]

$$\lambda' = \lambda_{\text{P}} + \frac{1}{3} V^{\text{G}} \lambda' \left[\frac{\lambda_{\perp,\text{G}} - \lambda_{\text{P}}}{\lambda' + k_z(\lambda_{\perp,\text{G}} - \lambda')} + \frac{2(\lambda_{\parallel,\text{G}} - \lambda_{\text{P}})}{\lambda' + k_x(\lambda_{\parallel,\text{G}} - \lambda')} \right] + \frac{3V^{\text{E}}\lambda'(\lambda_{\text{C}} - \lambda_{\text{P}})}{2\lambda' + \lambda_{\text{C}}} \quad (5)$$

$$k_x = \varepsilon(2 - 2\varepsilon^2)^{-1} \left[(1 - \varepsilon^2)^{-1/2} \cos^{-1} \varepsilon - \varepsilon \right] \quad (6)$$

$$k_z = 1 - 2k_x, \quad (7)$$

where $\lambda_{\perp,\text{G}}$ and $\lambda_{\parallel,\text{G}}$ represent the thermal conductivity of graphite along prism plane and basal plane, respectively; and V^{G} and V^{E} are the volume fractions of graphite and eutectic cementite.

3 Experiments

Six irons with different compositions were melted in a 500-kg medium-frequency induction furnace. High-quality steel scrap and pig iron were used as the charge. Ferromolybdenum, ferromanganese, ferrosilicon and carburizer were added as needed. After superheating to 1500 °C, the liquid was transferred into a ladle with inoculant (3.4 wt.% Zr–FeSi) on the bottom. For each sample, an EN-1564 Type II mold was poured. The compositions are given in Table 3. Carbon equivalent (CE) is calculated by $\text{CE} = \text{C} + 1/3(\text{Si} + \text{P})$.

Disk specimens with a diameter of 12.5 mm and a thickness of 2.5 mm were cut and then were used to determine the thermal diffusivity (α) and heat capacity (c_p)

Table 3 Chemical composition of samples (wt.%)

Iron	C	Si	Mn	P	S	Mo	Cu	CE
SP-1	3.39	1.64	0.46	0.030	0.025	0.35	0.55	4.0
SP-2	3.58	1.20	0.51	0.029	0.026	0.24	0.54	4.0
SP-3	3.53	1.49	0.50	0.030	0.029	0.34	0.54	4.0
SP-4	3.54	1.64	0.50	0.026	0.027	0.44	0.53	4.1
SP-5	3.57	1.59	0.51	0.026	0.024	0.24	0.54	4.1
SP-6	3.67	1.41	0.51	0.028	0.029	0.34	0.55	4.2

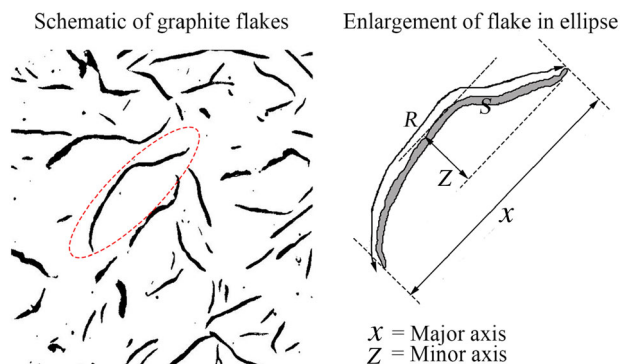


Fig. 2 Schematic showing characteristics of graphite flake

at room temperature using a NETZSCH LFA 457 laser flash apparatus. The density (d) was obtained by the Archimedes principle. And λ is calculated by:

$$\lambda = \alpha_c d. \quad (8)$$

The same specimens were then prepared for metallographic examination. The shape and area fraction of graphite were evaluated in an unetched condition by quantitative metallography with the software ImageJ Pro. The information on matrix was revealed by color etching technology. The color etchant was 50 g NaOH, and 4 g picric acid was dissolved in 100 mL distilled water. The etching procedure was carried out at 98 °C for 6 min. The volume fraction of eutectic cementite was obtained by counting point method.

The shape factor, ε , is one of the most important parameters for the prediction. Since the graphite flakes are usually lathy with slight bend, the approach shown in Fig. 2 was used to estimate the shape factor. The shape factor is approximated by:

$$\varepsilon = \frac{S}{\pi R^2}, \quad (9)$$

where R and S are the length and area of the graphite flake, respectively. Considering that most of the flakes cannot be displayed completely in a random 2-D section, the longest three flakes were selected and the average ε was calculated in each field of view; the average value of ten fields was taken as the final ε .

4 Results and discussion

4.1 Microstructure and thermal conductivity

Typical metallographic pictures of sample SP-2 are shown as examples in Fig. 3. Table 4 summarizes the information on microstructure and measured thermal conductivity. Each measurement was made on three different micrographs, and the average value was taken to improve the precision. It should be noted that only eutectic cementite is measured and tabulated as the fraction of cementite. Homogeneous structure, including fully pearlitic matrix and A-type graphite, was found for all the samples. As the result of analogous inoculation process, similar characteristic was also found in the shape factor of graphite. Differences mainly appear in the amount of graphite and thermal conductivity. This could be expected since both of them are determined by chemical composition. It can also be found that the graphite fractions of SP-2 to SP-5 are similar due to similar C content. And the difference in thermal conductivity of them can be explained by the addition of various alloying elements (Si and Mo).

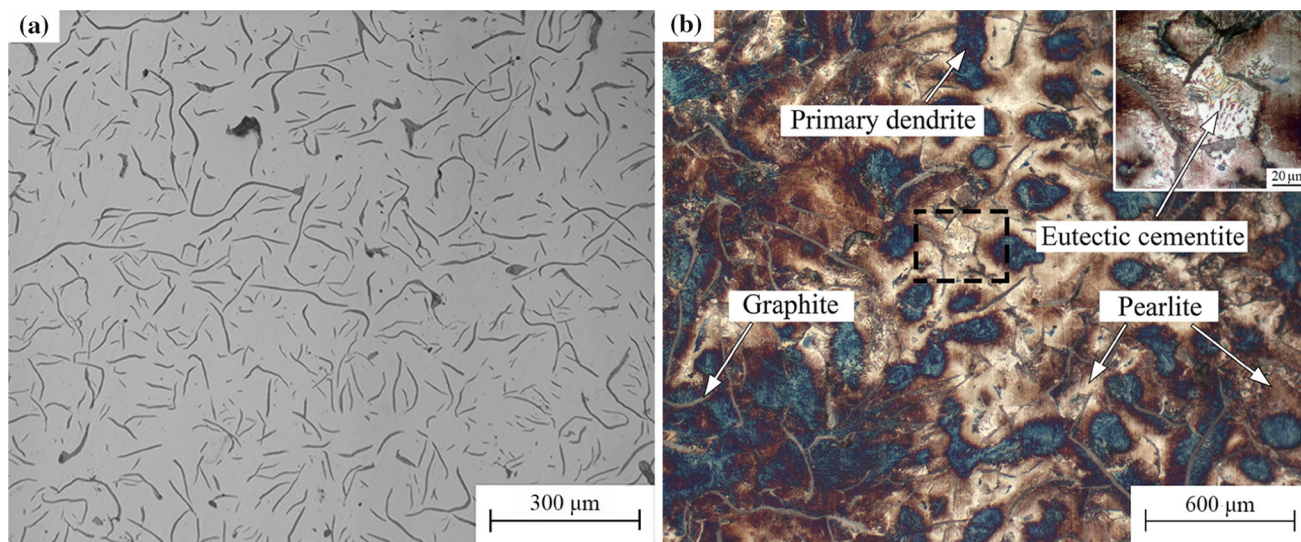


Fig. 3 Examples of optical images on unetched (a) and etched (b) sample SP-2

Table 4 Microstructural information and thermal conductivity (at room temperature) of samples

Iron	Matrix type	Graphite form		VGM ^a /10 ⁻²	VEM ^a /10 ⁻³	$\lambda/(W m^{-1} K^{-1})$
		Type	Shape factor			
SP-1	Fully pearlite	A	0.019 ± 0.004	8.9 ± 3	9.6 ± 0.8	47.8
SP-2	Fully pearlite	A	0.020 ± 0.006	9.7 ± 5	9.0 ± 0.7	54.1
SP-3	Fully pearlite	A	0.023 ± 0.003	9.5 ± 6	8.1 ± 2.0	50.2
SP-4	Fully pearlite	A	0.021 ± 0.004	9.3 ± 3	11.0 ± 2.0	51.4
SP-5	Fully pearlite	A	0.022 ± 0.002	9.6 ± 4	5.0 ± 1.0	52.4
SP-6	Fully pearlite	A	0.020 ± 0.003	10.5 ± 3	5.6 ± 1.0	55.7

^aVGM and VEM represent the measured volume fraction of graphite and eutectic cementite, respectively

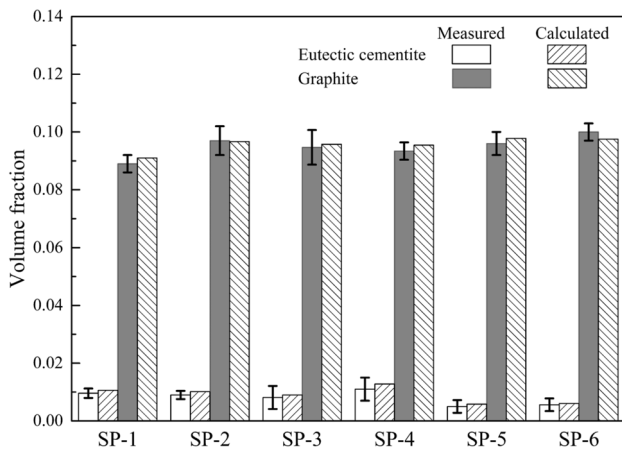


Fig. 4 Comparison of graphite and eutectic cementite fraction between experiments and calculations (error bars are ± 1 standard deviation)

The simulations were then performed using practical compositions and average shape factor $\varepsilon = 0.02$. Comparison between the predicted microstructure information and the measurements is shown in Fig. 4. Similar trends were found for predictions and experiments. In the presence of alloying elements, the graphite fraction does not have a strict linear relation with CE, and the calculations provide a very good agreement with the measurements. It seems that the calculation slightly overestimates the fraction of eutectic cementite. This suggests that the practical transformation during the end of solidification is more complex than the thermodynamic approximation. It is indeed expected since the micro-segregation and the accumulation of exotic impurity could lead to the complex non-equilibrium transformations during the end of solidification. Fortunately, such eutectic cementite is always in a low fraction by an effective inoculation, and thus the effects on total thermal conductivity are indeed slight.

Table 5 Calculated thermal conductivity of ferrite and pearlite

Thermal conductivity	SP-1	SP-2	SP-3	SP-4	SP-5	SP-6
$\lambda_F/(W m^{-1} K^{-1})$	31.33	32.37	30.77	31.42	35.85	32.90
$\lambda_P/(W m^{-1} K^{-1})$	26.65	27.41	26.24	26.72	29.93	27.80

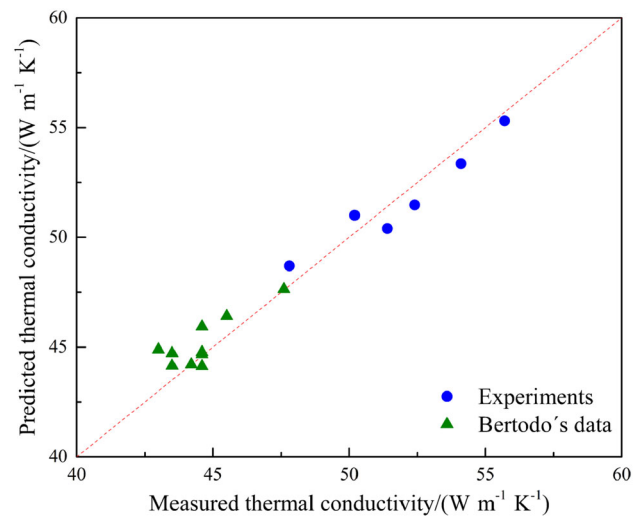


Fig. 5 Comparison between measured and predicted thermal conductivity

The calculated thermal conductivities of ferrite and pearlite are given in Table 5. Comparing with pure ferrite, it is clear that alloy addition significantly decreases the thermal conductivity of ferrite. The total calculated thermal conductivities are compared with experimental values measured in this work (as shown in Fig. 5). With the intention of expanding the comparison of the present model and practical measurements, comparisons between the measured data reported by Bertodo [26] and corresponding

Table 6 Experimental data measured by Bertodo [26] and corresponding calculated information

Composition	Matrix type	Graphite form		Measured $\lambda/(W m^{-1} K^{-1})$	Calculated $\lambda'/(W m^{-1} K^{-1})$
		Type	ε^b		
Plain (grade 17) ^a	Fully pearlite	A	0.032	47.6	47.64
Plain (grade 20) ^a	Fully pearlite	A	0.040	45.5	46.42
0.5 wt.% Mo	Pearlite, < 5% ferrite	A	0.032	44.6	44.67
0.5 wt.% Mo 1.0 wt.% Cu	Pearlite, < 5% ferrite	A	0.032	44.6	44.13
0.4 wt.% Mo 1.3 wt.% Ni	Pearlite, < 5% ferrite	A	0.032	44.2	44.21
2.2 wt.% Cu	Fully pearlite	A	0.040	43.5	44.72
1.0 wt.% Ni 0.3 wt.% Cr	Pearlite, < 1% ferrite	A	0.032	43.5	44.15
1.5 wt.% Cu 1.5 wt.% Ni	Fully pearlite	A	0.032	43.0	44.89
0.4 wt.% Cr	Pearlite, < 1% ferrite	A	0.032	44.6	45.94
0.4 wt.% Mo 0.4 wt.% Cr	Pearlite, < 5% ferrite	A	0.040	44.6	44.77

^aComposition of grade 17 and 20 is similar: 3.00–3.15 wt.% C, 1.67–1.75 wt.% Si and 0.6–0.8 wt.% Mn. And the mean values were taken to the calculation

^b ε was measured on the basis of ASTM A-247, since the graphite size was provided in the manner of ASTM classification by Bertodo

calculations are also provided in Fig. 5. Bertodo's measurements, including microstructural information and measured thermal conductivity, and corresponding results calculated by the present model are given in Table 6. Higher CE and longer graphite size make the thermal conductivities in the present work higher than Bertodo's data. However, as shown in Fig. 5, it is also clear that alloying elements play an important role in determining the thermal conductivity of gray cast iron, since carbon equivalents and shape factors are similar in either present experiments or Bertodo's results. Good agreement between the measured values and those calculated by the model is shown in Fig. 5. The small differences observed can be mainly explained by the simplifications in the measurement of shape factor and neglecting of the influence of MnS and additional intermetallic phases. More accurate value of the thermal properties of various microconstituents can also improve the precision of calculation. Within an acceptable error, the present model can be confirmed as a reasonable method to predict the thermal conductivity of pearlitic gray cast iron.

4.2 Influence of alloying elements on thermal conductivity

On the basis of the model explained above, the influence of alloying elements is discussed in this section. Since alloy additions affect the thermal conductivity of gray iron, mainly through solid solution with iron or promoting carbide formation [6], all the calculations were carried out under the assumption of the same shape factor ($\varepsilon = 0.02$).

Figure 6 illustrates the influence of alloying element i in the ternary system Fe-3.5 wt.% C- i . The situation of high Mo content is neglected since it may generate overmuch molybdenum carbides, whose thermal properties are unknown. For precipitated phases, the addition of Si, Mn, Cu or Ni increases the fraction of graphite in varying degrees and causes no precipitation of eutectic cementite. On the contrary, Mo decreases the fraction of graphite and promotes the precipitation of eutectic cementite. For the conduction of pearlite, all the additions of elements result in the reduction in thermal conductivity. This was indeed expected due to the existence of scattering of alloying atoms. Difference mainly appears at the extent of reduction. It can be found in Fig. 6b that the increasing Si content significantly decreases the thermal conductivity of pearlite, while the effect of Mo is the slightest. The curves of Mn, Cu and Ni lie within the Si and Mo curves. These can be explained by the difference of relative coefficients, molar mass and concentration between various elements. Finally, as shown in Fig. 6c, the addition of alloying elements, especially Si, reduces the total thermal conductivity, even though some of them improve the graphite fraction. It also suggests that Mo and Mn have the least impact on the thermal conductivity of pearlitic gray cast iron.

Considering that alloy strengthening also plays an important role in the resistance to thermal stress, the present model can be considered as a precise solution to obtain an optimal strength and thermal conductivity. For example, since it has been reported that there is a correlation between Mo content and tensile strength [27, 28], the calculation shown in Fig. 7 can be used to choose a suitable composition for various required properties.

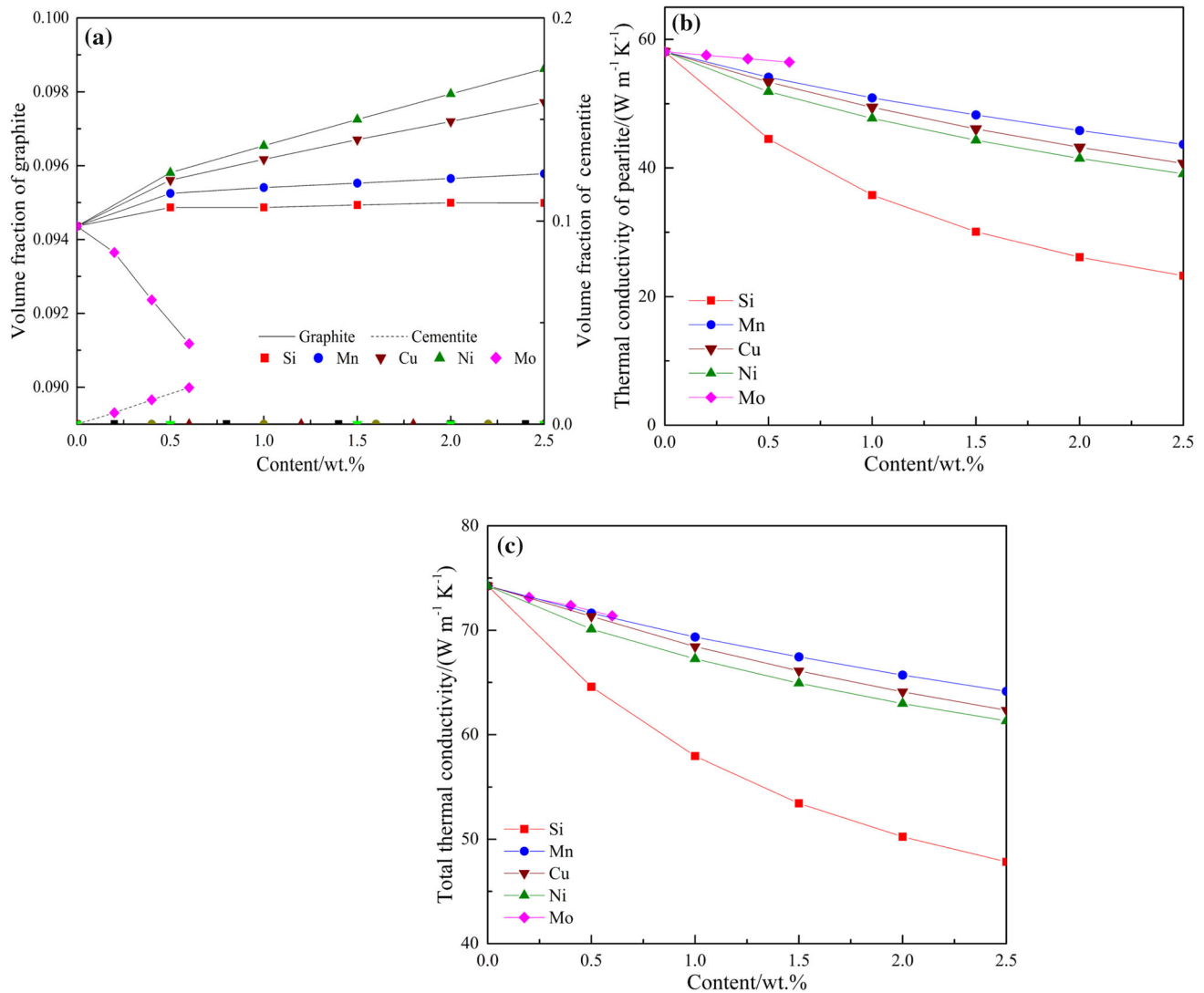


Fig. 6 Computational results showing influence of alloying elements i in Fe-C- i system on graphite fraction (a), thermal conductivity of pearlite (b) and total thermal conductivity (c)

5 Conclusions

1. A quantitative model was built to calculate the effects of alloying elements on the thermal conductivity of pearlitic gray cast iron. The microstructural information, including the fractions and concentrations of phases, was predicted by computational thermodynamics combining with micro-segregation. Depending on these results, the thermal conductivity was then estimated by the effective medium theory.
2. The calculation results were compared with experimental measurements, including graphite fraction, eutectic cementite fraction and thermal conductivity at room temperature. There is a good agreement between predictions and experimental data.
3. On the basis of calculation, the influence of Si, Mn, Mo, Cu and Ni on the structural constituents and thermal conductivity in a ternary system was discussed in detail. To various degrees, the addition of alloying elements always causes the reduction in thermal conductivity. However, combined with relative strengthening effects, the present model can also be used as the fundament for designing gray cast iron with high strength and high thermal conductivity.

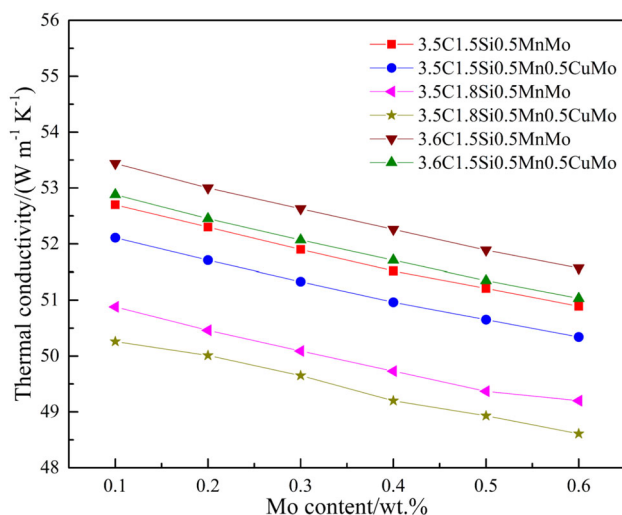


Fig. 7 Calculations showing relationship between thermal conductivity and Mo content for various compositions

References

- [1] F. Szymka, A. Oudin, *Int. J. Fatigue* 53 (2016) 82–91.
- [2] P. Lan, J.Q. Zhang, *Mater. Des.* 54 (2014) 112–120.
- [3] F. Bagnoli, F. Dolce, M. Bernabei, *Eng. Fail. Anal.* 16 (2009) 152–163.
- [4] G.M.C. Güiza, W. Hormaza, A.R. Galvis, L.M.M. Moreno, *Eng. Fail. Anal.* 82 (2017) 138–148.
- [5] X. Ding, H. Huang, W. Matthias, S. Huang, Y. Lu, Q. Feng, *Metall. Mater. Trans. A* 49 (2018) 3173–3177.
- [6] M.C. Rukadikar, G.P. Reddy, *J. Mater. Sci.* 21 (1986) 4403–4410.
- [7] R.L. Hecht, R.B. Dinwiddie, H. Wang, *J. Mater. Sci.* 34 (1999) 4775–4781.
- [8] D. Holmgren, I.L. Svensson, *Int. J. Cast Metal. Res.* 18 (2005) 321–330.
- [9] D. Holmgren, R. Kallbom, I.L. Svensson, *Metall. Mater. Trans. A* 38 (2007) 268–275.
- [10] M. Moonesan, A.H. Raouf, F. Madah, A.H. Zadeh, *J. Alloy. Compd.* 520 (2012) 226–231.
- [11] M. Chisamera, I. Riposan, S. Stan, C. Militaru, I. Anton, M. Barstow, *J. Mater. Eng. Perform.* 21 (2012) 331–338.
- [12] L. Collini, G. Nicoletto, R. Konecna, *Mater. Sci. Eng. A* 488 (2008) 529–539.
- [13] D. Holmgren, *J. Cast Metal. Res.* 18 (2005) 331–345.
- [14] M. Selin, M. Konig, *Metall. Mater. Trans. A* 40 (2009) 3235–3244.
- [15] J. Helsing, G. Grimvall, *J. Appl. Phys.* 70 (1991) 1198–1206.
- [16] T. Kraft, Y.A. Chang, *JOM* 49 (1997) 20–28.
- [17] H.T. Angus, *Cast iron: physical and engineering properties*, 2nd ed., Butterworth, London, UK, 1976.
- [18] Q. Chen, B. Sundman, *Mater. Trans.* 43 (2002) 551–559.
- [19] M. Hiller, *Phase equilibria, phase diagrams and phase transformations*, 2nd ed., Cambridge University Press, New York, USA, 2008.
- [20] T. Koshikawa, C.A. Gandin, M. Bellet, H. Yamamura, M. Bobadilla, *ISIJ Int.* 54 (2014) 1274–1282.
- [21] R.K. Williams, D.W. Yarbrough, J.W. Masey, T.K. Holder, R.S. Graves, *J. Appl. Phys.* 52 (1981) 5167–5175.
- [22] D. Korn, H. Pfeifle, J. Niebuhr, *Z. Phys. B Con. Mat.* 23 (1976) 23–26.
- [23] Y. Terada, K. Ohkubo, T. Mohri, T. Suzuki, *ISIJ Int.* 42 (2002) 322–324.
- [24] R.K. Williams, R.S. Graves, F.J. Weaver, D.W. Yarbrough, *J. Appl. Phys.* 62 (1987) 2778–2783.
- [25] A. Fert, I.A. Campbell, *J. Phys. F Met. Phys.* 6 (1976) 849–871.
- [26] R. Bertodo, *J. Strain Anal. Eng.* 5 (1970) 98–109.
- [27] W. Xu, M. Ferry, Y. Wang, *Mater. Sci. Eng. A* 390 (2005) 326–333.
- [28] X. Ding, X. Li, H. Huang, W. Matthias, S. Huang, Q. Feng, *Mater. Sci. Eng. A* 718 (2018) 483–491.